Research Square

Preprints are preliminary reports that have not undergone peer review.
They should not be considered conclusive, used to inform clinical practice,
or referenced by the media as validated information.

Comparative Evaluation and Uncertainty Analysis of Depth–Damage Functions for Flood Loss Estimation Using 2D Hydraulic Modelling

Hossein Salehi

ho.salehi67@gmail.com

Lorestan University

Naser Tahmasebipour

Lorestan University

Hossein Zeinivand

Lorestan University

Research Article

Keywords: Flood damage assessment, Depth–damage function, CCHE2D, Hydrodynamic modelling, Monetary loss estimation, Poldokhtar, Iran

Posted Date: November 2nd, 2026

DOI: https://doi.org/10.21203/rs.3.rs-11257776/v1

License: This work is licensed under a Creative Commons Attribution 4.0 International License.
Read Full License

Additional Declarations: No competing interests reported.

Comparative Evaluation and Uncertainty Analysis of Depth–Damage Functions for Flood Loss Estimation Using 2D Hydraulic Modelling

Hossein Salehi[1*], Naser Tahmasebipour[2], Hossein Zeinivand[3]

[1] Department of Watershed Management Engineering, Lorestan University, Khorramabad, Lorestan, Iran

[2] Department of Watershed Management Engineering, Lorestan University, Khorramabad, Lorestan, Iran

[3] Department of Watershed Management Engineering, Lorestan University, Khorramabad, Lorestan, Iran

[*]Corresponding author: Hossein Salehi, E-mail: ho.salehi67@gmail.com

ORCID: Hossein Salehi [0000-0001-7533-4556]; Naser Tahmasebipour [0000-0003-1729-5135]; Hossein Zeinivand [0000-0003-3132-9194]

Acknowledgments: The authors gratefully acknowledge the Regional Water Company for providing the necessary data and information used in this research.

Abstract

Flood-induced economic losses in data-scarce regions are difficult to quantify reliably because hydraulic modelling, depth–damage relationships, and building-exposure data are rarely combined within a single, locally calibrated framework. This study developed an integrated methodology for estimating residential flood damage in the Poldokhtar urban floodplain on the Kashkan River, western Iran, a reach that experienced severe inundation in 2016 and 2019. The two-dimensional CCHE2D model was calibrated and validated against surveyed cross-sections and 30 field control points, achieving a velocity RMSE of 0.075 m s^{-1} and no statistically significant difference between simulated and observed flood depths (paired t-test, $p = 0.718$). Four candidate depth–damage functions — two exponential forms, a piecewise linear function, and a cubic polynomial — were fitted to locally observed damage data; the exponential function S2 ($Y = 1 - \exp(-0.94x)$) provided the best performance (RMSE = 11.05%, MAE = 8.41%, CC = 0.96). Three approaches for converting relative damage into monetary loss were compared, showing that spatially disaggregated building information (Approach A2) reduced the relative error to 6.4%, compared with 31.1% and 41.3% for approaches based on generalized building values, and that a fixed regional recovery coefficient performed adequately only at shallow depths. A McNemar test further revealed a statistically significant asymmetry between simulated and satellite-derived flood extents ($\chi^2 = 14.02$, $p = 0.00018$). The results demonstrate that coupling calibrated hydraulic simulation with locally derived depth–damage functions and spatially explicit exposure data substantially improves flood-loss estimation accuracy, offering a transferable framework for flood-risk assessment in other data-scarce Iranian floodplains.

Keywords: Flood damage assessment; Depth–damage function; CCHE2D; Hydrodynamic modelling; Monetary loss estimation; Poldokhtar, Iran

1. Introduction

Floods are among the most damaging natural hazards worldwide, generating substantial losses to settlements, infrastructure, economic activities, and ecosystems. The scale of flood impacts is influenced not only by the magnitude and frequency of precipitation events but also by topography, drainage characteristics, land use, sediment dynamics, and the spatial distribution of exposed assets. In semi-arid and mountainous environments, intense rainfall can rapidly generate surface runoff and sediment transport, increasing the geomorphic and hydraulic consequences of flooding. Recent research in Iranian catchments has demonstrated the relationship between rainfall erosivity and sediment yield, highlighting the role of precipitation characteristics in controlling erosion and sediment production at the catchment scale (Tajbakhshian et al. 2024). Similar studies have emphasized the importance of integrating spatial environmental information and erosion susceptibility assessment for understanding the response of semi-arid basins to rainfall and runoff processes (Ait Haddou et al. 2024).

Iran is particularly susceptible to flash flooding because of its complex mountainous terrain, spatially variable precipitation regime, and concentration of settlements and infrastructure along river corridors. The interaction between intense rainfall, steep topographic gradients, channel morphology, and floodplain occupation can produce rapid changes in flow depth and inundation extent. Riverine processes are further influenced by sediment transport and water-quality characteristics. For example, Radmehr et al. (2024) documented the relationship between sediment characteristics, heavy-metal contamination, and hydrogeochemical properties in the Mashalak River, demonstrating the broader environmental significance of river processes in Iranian catchments. Such interactions are particularly relevant in western Iran, where active river systems and narrow floodplains create substantial exposure to flood hazards.

The Kashkan River basin in Lorestan Province represents one of the important flood-prone environments in western Iran. The city of Poldokhtar is located near the confluence of the Kashkan and Seimareh rivers and occupies a relatively

narrow floodplain downstream of the Tang-e Poldokhtar gorge. The city has experienced severe flooding, including major events in 2016 and 2019. The March-April 2019 flood caused extensive inundation and substantial damage to residential areas, infrastructure, and public services. A detailed post-disaster investigation reported severe impacts on several neighbourhoods of Poldokhtar and documented widespread flood deposits and building damage following the event (Maarefvand et al. 2021). Recent spatial flood-susceptibility research on the Kashkan River has further identified the Poldokhtar region as a highly vulnerable part of the basin and demonstrated the usefulness of integrating river morphology with spatial susceptibility modelling (Ghahraman et al. 2023). These characteristics make the Poldokhtar floodplain a suitable natural laboratory for investigating the relationship between flood hydraulics, spatial exposure, and economic damage.

Accurate estimation of flood-induced economic losses requires reliable characterization of both the flood hazard and the vulnerability of exposed assets. Hydrodynamic modelling provides the physical basis for estimating variables such as water depth, flow velocity, inundation extent, and flood duration. Two-dimensional models are particularly useful in complex floodplains because they can represent spatial variations in flow direction and hydraulic conditions that are difficult to capture with one-dimensional formulations. The CCHE2D model, developed at the National Center for Computational Hydroscience and Engineering, is a two-dimensional numerical model capable of simulating free-surface flow and sediment transport in natural and engineered channels. Its application to meandering channels has demonstrated its ability to represent spatial variations in velocity, water level, and flow structure associated with channel curvature The CCHE2D model, developed at the National Center for Computational Hydroscience and Engineering, is a two-dimensional depth-averaged model capable of simulating free-surface flow, sediment transport and morphological change in natural rivers (Jia and Wang 1999). Its application to Iranian rivers has demonstrated its usefulness for analysing complex flow patterns in straight and meandering reaches (Salmasi et al. 2020).

The spatial representation of environmental and geomorphological conditions is another important component of flood-hazard assessment. Remote sensing and GIS have increasingly been used to identify and map natural hazards by integrating topography, land cover, geological conditions, drainage characteristics, and other spatial variables. For example, Khodaei Geshlag et al. (2020) demonstrated the application of Landsat imagery to post-earthquake landslide mapping in northwestern Iran, while more recent work has combined GIS-based spatial analysis with multi-criteria approaches to produce susceptibility maps for natural hazards (Taher et al. 2025). Although these studies address hazards other than flooding, their methodological relevance lies in the use of spatially distributed environmental information to characterize heterogeneous hazard conditions. Similar GIS-based approaches have also been applied to erosion and sediment-yield assessment in Iranian drainage basins (Amini et al. 2010; Tajbakhshian et al. 2024).

Hydrodynamic modelling alone, however, does not provide an estimate of economic loss. Flood damage assessment commonly relies on depth-damage functions (DDFs), which express the expected proportion of damage to an asset as a function of inundation depth. These functions provide a link between hydraulic model outputs and estimates of physical or monetary damage and have been incorporated into established flood-risk assessment frameworks, including the U.S. Army Corps of Engineers' Hydrologic Engineering Center Flood Impact Analysis (HEC-FIA) system. Despite their widespread use, DDFs remain associated with substantial methodological uncertainty because damage relationships vary with building characteristics, construction materials, occupancy type, flood characteristics, and socioeconomic conditions. Poulose and Kumar (2024), for example, identified differences in flooded-depth calculation, damageable value interpretation, and occupancy-specific replacement costs as important sources of variation in flood-loss estimates obtained using HEC-FIA and alternative approaches.

The definition of the damage initiation point is another important source of uncertainty. Rahim et al. (2024) demonstrated that the assumed damage initiation point of a depth-damage function can substantially affect flood-risk estimates, particularly when damage is assumed to begin below the first-floor elevation. This finding is important for urban floodplains where relatively shallow inundation may affect buildings differently depending on floor elevation,

construction type, and the location of vulnerable building components. Consequently, the selection and formulation of DDFs should be considered together with the characteristics of the exposed building stock and the hydraulic conditions generated by the flood model.

The transferability of depth-damage functions between different geographical and socioeconomic settings represents a further challenge. Many commonly used functions were developed from empirical data collected in North America, Europe, or other regions with building standards, construction practices, asset values, and flood-response conditions that differ from those found in Iran. Applying such functions without local validation can therefore introduce uncertainty into both relative and monetary damage estimates. Paulik et al. (2023) demonstrated that residential building damage models can vary according to flood type and local damage characteristics, emphasizing the importance of context-specific information when transferring damage relationships between different hazard environments. In Iran, the limited availability of empirical post-flood damage datasets makes this issue particularly relevant, increasing the need for approaches that explicitly account for local building and economic characteristics.

The conversion of relative damage into monetary loss introduces another level of uncertainty. Monetary estimation requires information on the value of exposed assets, building floor area, construction or replacement costs, and, where appropriate, regional recovery coefficients. The use of average property values or uniform floor-area assumptions can obscure substantial differences among individual buildings and neighbourhoods. Spatially disaggregated building information can provide a more realistic representation of exposure by linking hydraulic conditions to the actual size and location of individual assets. This approach is particularly relevant in heterogeneous urban floodplains such as Poldokhtar, where residential, commercial, and administrative structures are distributed within a relatively confined flood-prone area.

The Poldokhtar floodplain therefore provides an appropriate setting for integrating two-dimensional hydraulic modelling with spatially explicit flood-damage assessment. The combination of a complex meandering river system, a narrow floodplain, heterogeneous urban development, and documented severe flooding provides an opportunity to examine how hydraulic characteristics are translated into building-level damage and monetary loss. Previous studies of the Kashkan basin have primarily focused on flood susceptibility, geomorphological characteristics, or environmental processes, whereas a systematic evaluation of alternative depth-damage formulations coupled with high-resolution CCHE2D hydraulic outputs remains limited.

Accordingly, this study develops an integrated framework for flood-damage estimation in the Poldokhtar urban floodplain. First, flood inundation depth and extent are simulated using the CCHE2D two-dimensional hydrodynamic model and evaluated against available observations. Second, alternative depth-damage formulations, including two exponential functions, a piecewise linear function, and a cubic polynomial function, are compared for estimating relative damage to residential buildings. Third, the influence of spatially disaggregated building floor areas and regional recovery cost coefficients on monetary damage estimates is evaluated within the HEC-FIA framework. The resulting approach combines hydraulic modelling, geomorphological and spatial analysis, and economic damage assessment to provide a locally informed framework for flood-loss estimation in data-scarce flood-prone regions of western Iran.

2. Materials and Methods

2.1. Study Area

The study was conducted in Poldokhtar, located in Lorestan Province, western Iran, along the Kashkan River. The investigated reach covers the river corridor extending from the upstream entrance to the downstream exit of Poldokhtar city. The urban area is characterized by a close spatial relationship between the river channel, floodplain, residential

buildings, agricultural land, and other developed surfaces. This configuration makes the spatial distribution of flood depth particularly important for reliable damage estimation.

Poldokhtar has experienced recurrent flooding, with the April 2019 flood representing one of the most significant recent events in the region. During this event, extensive areas of the urban fabric and surrounding floodplain were inundated. Therefore, the area provides an appropriate case study for examining the relationship between simulated flood depth and observed building damage, particularly under conditions in which the spatial variability of exposed assets is considerable.

2.2. Data and General Methodological Framework

The methodology consisted of three interconnected components: hydraulic simulation, development of localized depth-damage relationships, and conversion of estimated damage ratios into monetary losses. The overall framework was designed so that the hydraulic model supplied spatially distributed flood depth information, while field observations and spatially detailed socioeconomic data were used to develop and evaluate the damage estimation procedure.

The hydraulic component was based on the two-dimensional CCHE2D model. The required topographic and hydraulic information included a digital elevation model, surveyed river cross-sections, observed discharge hydrographs, Manning's roughness coefficient, and boundary conditions. The observed hourly discharge data were obtained from the Poldokhtar hydrometric station for the flood events considered in this study. The computational domain and river geometry were prepared using topographic information and surveyed cross-sections.

For the damage assessment component, land-use information, building characteristics, observed damage information, and hydraulic outputs were integrated in a GIS environment. The economic database included the number of residential buildings, building floor area, agricultural land, and monetary values. Information at the statistical-block level was used together with field observations collected for 250 sampled buildings. The use of spatially differentiated building areas was intended to avoid the uncertainty associated with assigning a single average building size to the entire study area.

2.3. Two-Dimensional Hydraulic Simulation Using CCHE2D

CCHE2D was used to simulate the spatial distribution of flood flow and water depth throughout the study reach. The model was implemented using the CCHE-MESH preprocessing environment for generation of the computational grid and the CCHE-GUI environment for hydraulic simulation and visualization.

The computational geometry was constructed from the digital elevation data and surveyed cross-sections of the river reach. The upstream boundary condition was defined using the observed discharge hydrograph, whereas the downstream boundary was represented by the corresponding water-surface elevation. The Manning roughness coefficient was calibrated using observed hydraulic conditions.

Two computational grids, with dimensions of 1800 × 250 and 2500 × 350, were tested to evaluate the influence of spatial discretization on the simulated hydraulic variables. Model performance was assessed by comparing simulated and observed flow velocity and water depth at selected cross-sections.

The finer grid, with dimensions of 2500 × 350, combined with a Manning roughness range of 0.042–0.057, provided the lowest model error and was therefore selected as the optimal computational configuration for subsequent flood simulations. The selected configuration produced an RMSE of approximately 0.075 m s−1 for flow velocity, while the corresponding relative MAE (expressed as a percentage of measured velocity) was approximately 7.54%.

2.3.1. Hydraulic Model Validation

Model validation was performed using hydraulic observations that were not used in the calibration stage. Two additional sections along the study reach were selected for validation based on observed flow depth.

In addition to point-based comparison, the model was evaluated at 30 systematically selected control points within the inundated area. At each point, field-observed flood depth was compared with the corresponding CCHE2D output.

The statistical evaluation included the root mean square error (RMSE), mean absolute error (MAE), and paired-sample t-test. The paired test was used to determine whether the difference between observed and simulated flood depths was statistically significant. The analysis reported a two-tailed p-value of 0.718, indicating no statistically significant difference between the two sets of depth observations at the 95% confidence level.

The validated CCHE2D model was subsequently used to generate the spatially distributed flood-depth raster required for the damage assessment.

2.4. Development of Localized Depth-Damage Functions

The principal objective of this stage was to quantify the relationship between flood depth and the percentage of damage to residential buildings. Rather than directly adopting a generalized depth-damage relationship, locally observed damage information was used to evaluate several alternative functional forms.

Observed flood damage and corresponding flood depths were compiled for residential buildings affected by the flood. The observed information was then used to establish empirical relationships between flood depth, denoted by x, and relative damage, denoted by Y.

Here, Y represents the proportion of building damage, ranging from 0 to 1, while x represents flood depth in meters.

Four alternative formulations were evaluated.

2.4.1. Model S1: Exponential Function

$$Y = 1 - \exp(-x^{1.12})$$

This formulation represents a nonlinear increase in damage with increasing flood depth, with the damage ratio approaching 1 as flood depth increases.

2.4.2. Model S2: Exponential Function

$$Y = 1 - \exp(-0.94x)$$

The second exponential formulation was evaluated as an alternative representation of the observed depth-damage relationship. Similar to S1, the function approaches complete damage as flood depth increases.

2.4.3. Model S3: Piecewise Linear Function

For flood depths between 0.1 and 2.4 m:

$$Y = 0.21 + 0.33x$$

For flood depths greater than 2.4 m:

$$Y = 1$$

This formulation assumes a linear increase in damage within the observed intermediate-depth range and complete damage above the specified threshold.

2.4.4. Model S4: Cubic Polynomial Function

For flood depths between 0.1 and 4.5 m:

$$Y = 0.008 + 0.82x - 0.24x^2 + 0.024x^3$$

For depths greater than 4.5 m:

$$Y = 1$$

The four functions and their applicable depth ranges were derived from the locally observed depth-damage data.

2.5. Evaluation of Depth-Damage Functions

The performance of the four depth-damage functions was evaluated by comparing calculated damage ratios with observed damage ratios. Three statistical criteria were used: the root mean square error (RMSE), mean absolute error (MAE), and correlation coefficient (CC).

The RMSE was calculated as:

$$\mathrm{RMSE} = \sqrt{\frac{1}{n}\sum\left(Y_i - \hat{Y}_i\right)^2}$$

where Y_i is the observed damage ratio, $\hat{Y}_i$ is the damage ratio estimated by the fitted function, and n is the number of observations.

The MAE was calculated as:

$$\mathrm{MAE} = \frac{1}{n}\sum\left|Y_i - \hat{Y}_i\right|$$

The correlation coefficient was used to quantify the degree of association between observed and estimated damage values.

The function providing the lowest prediction error while maintaining a strong correlation with observed damage was retained as the basis for subsequent monetary loss estimation.

2.6. Conversion of Relative Damage to Monetary Loss

After determining the relationship between flood depth and relative building damage, the estimated damage ratios were converted into monetary losses.

A major source of uncertainty in monetary flood-damage estimation is the estimation of the value of exposed buildings. To investigate this issue, three alternative approaches for assigning monetary building values were compared. The first approach relied on a generalized or average building size, whereas the spatially explicit approach used information at the statistical-block level. This distinction allowed the effect of spatial variability in building floor area to be evaluated.

The economic information incorporated the number of residential buildings, building floor area, and monetary values obtained from statistical-block data and field surveys. Field information was collected for 250 sampled buildings. These data were integrated with the spatial flood-depth outputs generated by CCHE2D.

For each exposed building, the estimated monetary damage was calculated as:

$$D_i = V_i \times Y(x_i)$$

where D_i is the estimated monetary damage to building i, V_i is the monetary value assigned to that building, and $Y(x_i)$ is the damage ratio corresponding to the simulated flood depth x_i.

This spatially explicit procedure allows buildings located within the same flood-depth class to have different monetary losses when their floor areas or monetary values differ.

2.7. Regional Recovery/Reconstruction Coefficient

To further examine the conversion of relative damage into monetary damage, a regional recovery/reconstruction coefficient, RC, was incorporated into the estimation procedure.

The coefficient was used to account for the difference between the total reconstruction cost of a building and the actual monetary loss associated with a particular flood depth. An RC value of 0.45 was adopted for the low-depth damage assessment considered in the study.

Accordingly, the monetary loss can be represented as:

$$D_i = Y(x_i) \times V_{r,i} \times \mathrm{RC}$$

where $V_{r,i}$ represents the estimated reconstruction or replacement value of building i.

The performance of the RC-based approach was examined separately for different flood-depth ranges. The analysis considered depths below 1 m, depths between 1 and 2.5 m, and depths greater than 2.5 m. The purpose was to determine whether a single conversion approach performs consistently across different levels of flood severity.

2.8. Integration of CCHE2D Outputs with Damage Functions

The final damage-estimation procedure was based on the spatial integration of the CCHE2D flood-depth map with the residential exposure database and the selected depth-damage functions.

For each spatial unit or building, the simulated flood depth was extracted from the CCHE2D output. The corresponding relative damage ratio was then obtained from each candidate depth-damage function and combined with the spatially specific building value. Alternative monetary valuation procedures were subsequently applied, and the estimated monetary damage was compared with observed or field-assessed losses.

This procedure allowed the study to distinguish between two sources of uncertainty: uncertainty associated with the functional form of the depth-damage relationship and uncertainty associated with the monetary valuation of exposed buildings.

2.9. Statistical Comparison of Monetary Damage Estimates

The final stage involved comparing the monetary losses estimated by the alternative models with observed damage values. The absolute relative error was used to assess the accuracy of the monetary estimates:

$$\mathrm{RE}_i = \left| \frac{D_{i,\mathrm{est}} - D_{i,\mathrm{obs}}}{D_{i,\mathrm{obs}}} \right| \times 100$$

where $D_{i,\mathrm{est}}$ is the estimated monetary damage and $D_{i,\mathrm{obs}}$ is the corresponding observed damage.

The analysis was conducted both for the complete dataset and for separate flood-depth intervals. This depth-stratified evaluation was important because the relationship between flood depth and building damage is nonlinear, and the performance of a monetary conversion method may change as flood severity increases.

3. Results

3.1. CCHE2D Model Calibration and Validation

The hydraulic simulations were first evaluated by examining the sensitivity of the model results to the computational grid and Manning's roughness coefficient. Two computational grids with dimensions of 1800 × 250 and 2500 × 350 were tested. The comparison of simulated and measured flow velocity and water depth at the available cross-sections showed that the 2500 × 350 grid provided a closer representation of the measured hydraulic conditions and

was therefore selected for the subsequent simulations. The selected configuration was associated with a Manning's roughness coefficient ranging from 0.042 to 0.057.

Table 1 Comparison of measured and simulated flow velocity for the tested computational grids

Cross-section	Measured velocity (m/s)	Simulated – 1800×250 (m/s)	Simulated – 2500×350 (m/s)
A	0.92	1.02	0.95
C	1.09	1.01	1.08
E	0.95	0.99	0.96
F	0.87	0.95	0.89
G	0.82	0.98	0.85

Table 2 Comparison of measured and simulated flow depth for the tested computational grids

Cross-section	Measured depth (m)	Simulated – 1800×250 (m)	Simulated – 2500×350 (m)
A	1.02	1.08	1.04
C	1.05	0.98	1.01
E	1.03	0.95	0.99
F	0.87	0.92	0.85
G	0.88	0.96	0.89

The comparison of the hydraulic variables showed that the finer computational grid provided improved agreement with the measured conditions. For the selected 2500 × 350 grid, the simulated flow velocities at the five calibration sections were close to the measured values. A similar pattern was observed for flow depth, supporting the selection of this grid for the flood simulations.

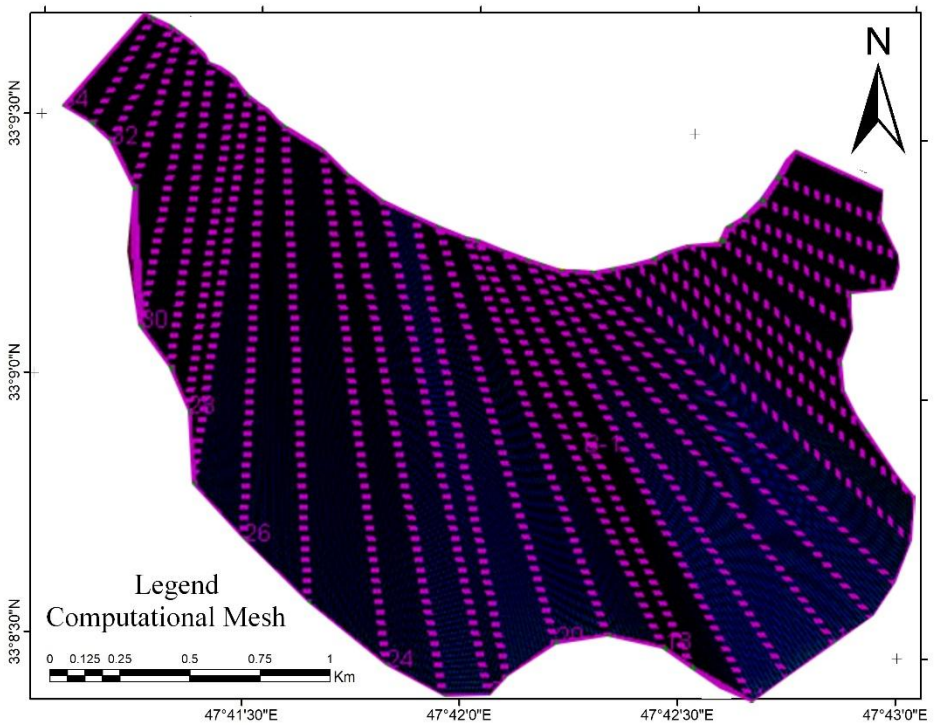


Fig. 1 Selected computational grid (mesh) and the surveyed cross-sections

The effect of Manning's roughness coefficient was subsequently examined for the candidate grid configurations. The results indicated that the combination of the 2500 × 350 computational grid and a Manning's roughness range of 0.042–0.057 provided the most suitable representation of the measured hydraulic conditions. The corresponding comparison of flow velocity and flow depth for different roughness ranges is presented below.

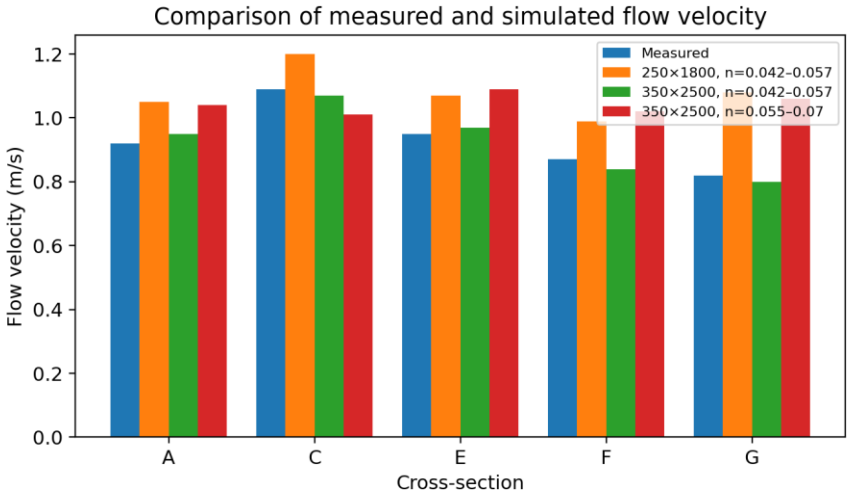


Fig. 2 Comparison of flow velocity under different computational-grid and roughness conditions

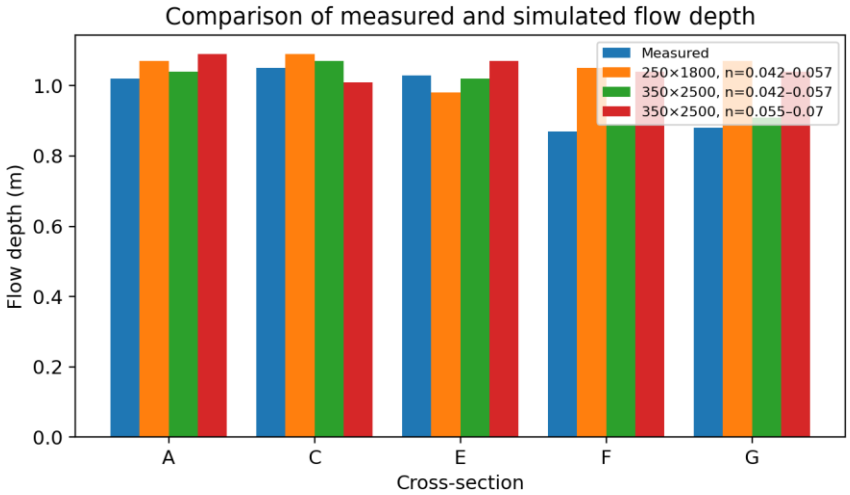


Fig. 3 Comparison of flow depth under different computational-grid and roughness conditions

For independent validation, the calibrated model was evaluated at two additional river cross-sections using measured and simulated flow depths. At section B, the measured and simulated depths were 1.04 and 1.02 m, respectively, whereas at section D they were 0.98 and 0.95 m, respectively. These results indicate a close correspondence between the modeled and observed hydraulic conditions at the validation sections.

Table 3 Validation of the CCHE2D model at independent cross-sections

Cross-section	Measured depth (m)	Model-simulated depth (m)
B	1.04	1.02
D	0.98	0.95

The model was also evaluated using 30 control points distributed within the inundated area. The mean observed flood depth was 3.25 m, while the corresponding mean simulated depth was 3.12 m. The mean difference between the paired observations was 0.13 m, with a standard deviation of 1.95 m. The paired t-test yielded $t = 0.365$ with 29 degrees of freedom and $p = 0.718$. The 95% confidence interval for the mean difference was approximately −0.598 to 0.858 m. Therefore, the observed and simulated flood depths did not show a statistically significant difference at the 95% confidence level.

Table 4 Statistical comparison of observed and simulated flood depths (paired t-test)

Statistic	Value
Number of control points (n)	30
Mean observed depth (m)	3.25
Mean CCHE2D-simulated depth (m)	3.12
Mean difference, $\bar{d}$ (m)	0.13
Standard deviation of differences, Sd (m)	1.95
Computed t	0.365
Critical t ($\alpha = 0.05$, df = 29)	2.045
Degrees of freedom (df)	29
p-value (two-tailed)	0.718
95% confidence interval of the difference (m)	−0.598 to 0.858

The error analysis further showed an RMSE of approximately 0.075 m s^{-1} for simulated flow velocity and a relative MAE (as a percentage of measured velocity) of approximately 7.54% for the selected model configuration. These results, together with the cross-section validation, provided the basis for using the calibrated CCHE2D model to generate spatially distributed flood-depth information for the subsequent damage assessment.

3.2. Simulated Flood Extent and Flood Depth

The calibrated CCHE2D model was used to simulate the flood conditions for the 2016 and 2019 events. The resulting flood-extent maps show the spatial distribution of inundated areas within the study reach. The corresponding flood-depth maps provide the spatially variable water depth required for the subsequent depth–damage analysis.

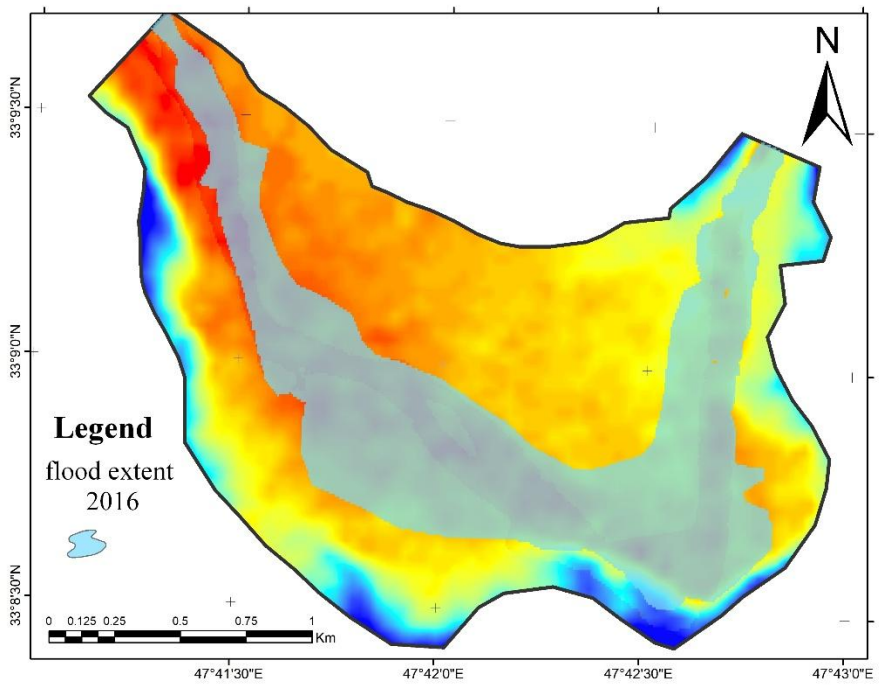


Fig. 4 Simulated flood extent for the 2016 event

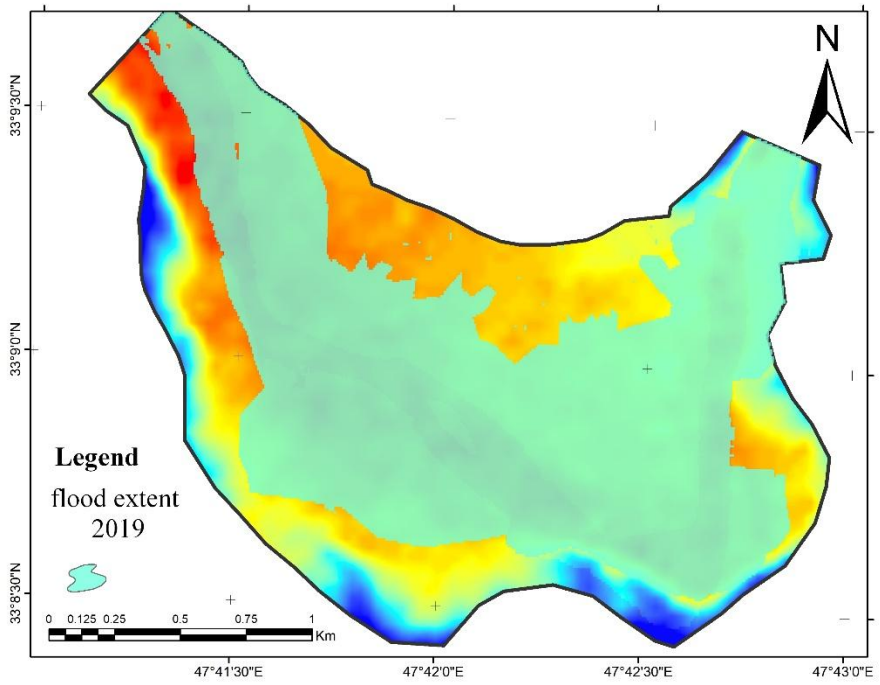


Fig. 5 Simulated flood extent for the 2019 event

The simulated flood-depth distribution for the two events is presented in the corresponding depth maps below. These maps were used as the hydraulic input for linking flood intensity to building damage.

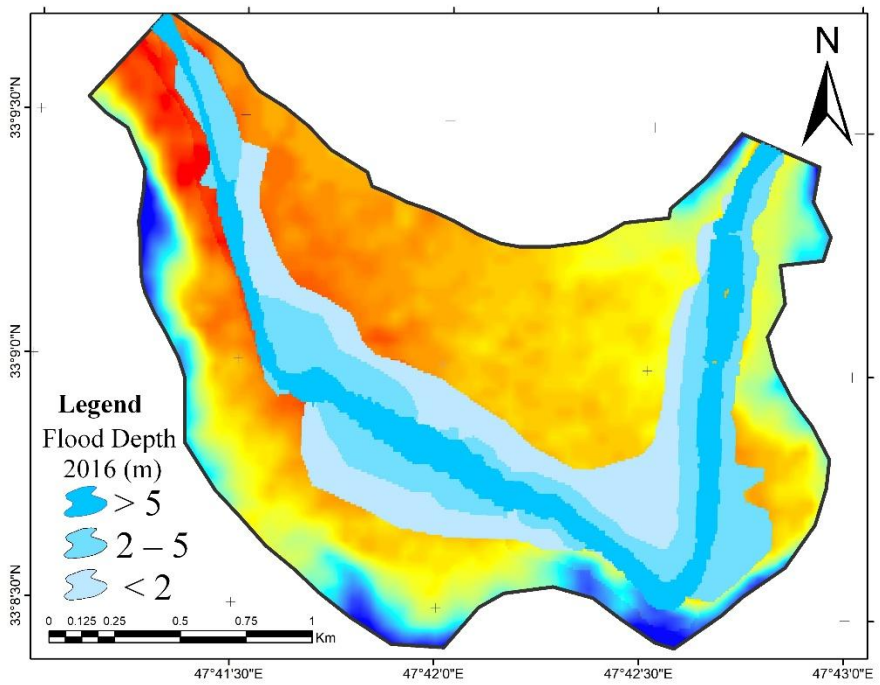


Fig. 6 Simulated flood-depth map for the 2016 event

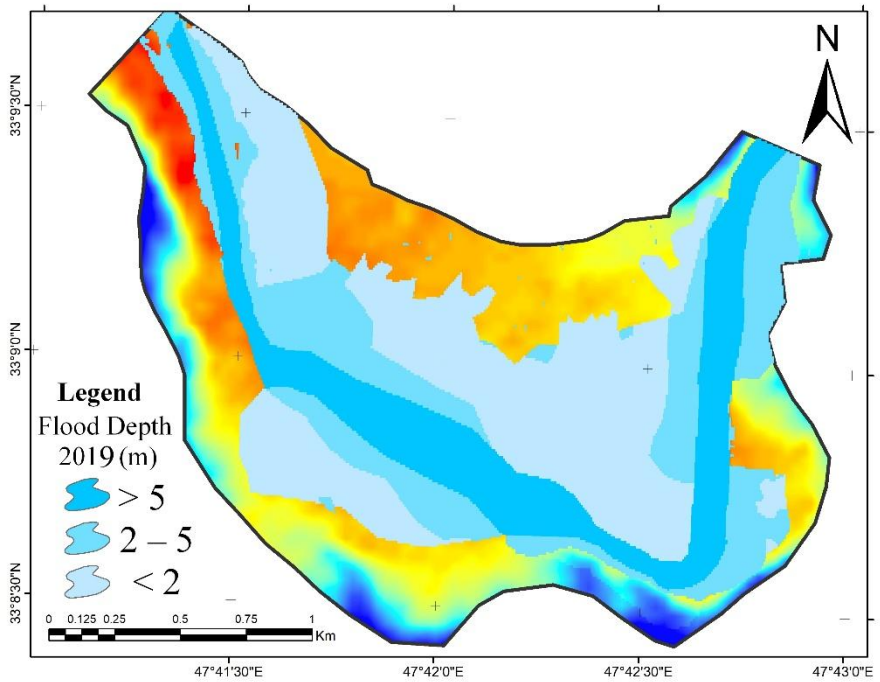


Fig. 7 Simulated flood-depth map for the 2019 event

3.3. Performance of the Local Depth–Damage Functions

Four candidate depth–damage functions were fitted to the observed flood-depth and building-damage data. The evaluated functions consisted of two exponential relationships, one piecewise linear function, and one cubic polynomial function. For the exponential functions, the damage fraction asymptotically approaches 1 as flood depth increases. In the piecewise linear formulation, the relationship was defined for depths from 0.1 to 2.4 m and a

damage level of 100% was assigned to greater depths. The fourth function used a cubic polynomial over the range of 0.1–4.5 m, with damage constrained to 100% beyond this range.

Table 5 Fitted depth–damage functions based on the observed depth–damage data

Model	Depth range x (m)	Function (Y = damage fraction, x = depth in m)
S1	≥ 0.1	$Y = 1 - \exp(-x^{1.12})$
S2	≥ 0.1	$Y = 1 - \exp(-0.94x)$
S3	0.1–2.4 / > 2.4	$Y = 0.21 + 0.33x$ / $Y = 1$
S4	0.1–4.5 / > 4.5	$Y = 0.008 + 0.82x - 0.24x^2 + 0.024x^3$ / $Y = 1$

The performance of the four functions was assessed using RMSE, MAE, and the correlation coefficient (CC). S1 produced an RMSE of 11.21%, an MAE of 9.02%, and a CC of 0.95. S2 produced an RMSE of 11.05%, an MAE of 8.41%, and a CC of 0.96. S3 yielded an RMSE of 11.45%, an MAE of 9.62%, and a CC of 0.91, while S4 resulted in an RMSE of 11.32%, an MAE of 9.24%, and a CC of 0.94.

Table 6 RMSE, MAE, and CC for the evaluated depth–damage functions

Model	RMSE (%)	MAE (%)	CC
S1	11.21	9.02	0.95
S2	11.05	8.41	0.96
S3	11.45	9.62	0.91
S4	11.32	9.24	0.94

The comparison demonstrates that all four functions showed a strong correlation with the observed damage data; however, the magnitude of prediction errors differed among the models. S2 produced the lowest RMSE and MAE and the highest CC among the four evaluated functions. The S2 relationship was therefore used as the selected local depth–damage function for the subsequent flood-loss estimation.

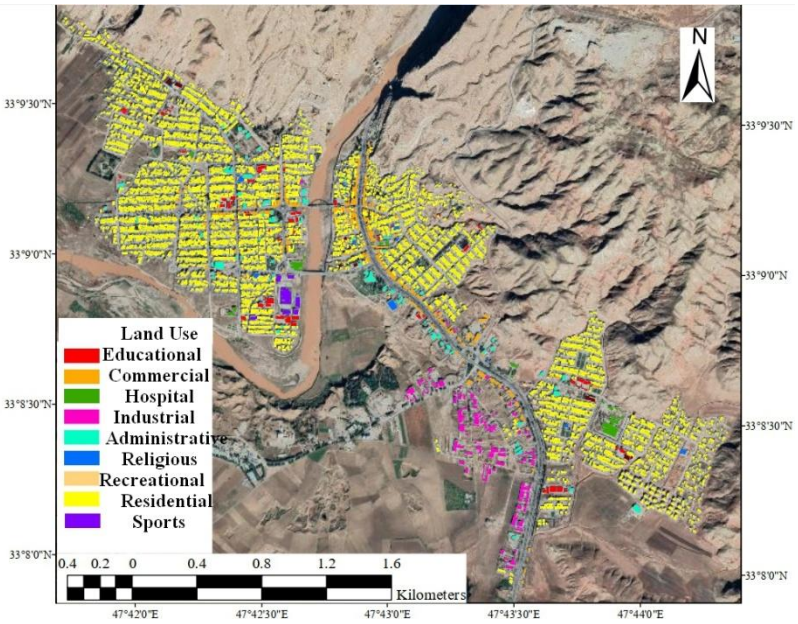
The selected S2 function was expressed as:

$$Y = 1 - \exp(-0.94x)$$

where x represents flood depth in meters and Y represents the damage fraction. The function was defined for flood depths equal to or greater than 0.1 m. The results demonstrate that the selected relationship provides a locally calibrated representation of the increase in relative building damage with increasing flood depth.

3.4. Spatial Representation of Buildings and Monetary Loss Estimation

Following the estimation of relative damage from flood depth, three alternative approaches were evaluated for converting relative building damage into monetary loss. Land-use information for the study area was obtained from Poldokhtar Municipality, while economic and building information was compiled using statistical-block data and field observations. Field information was collected for 250 sampled buildings.



363
364 **Fig. 8** Land-use map of the study area (source: Poldokhtar Municipality)



365

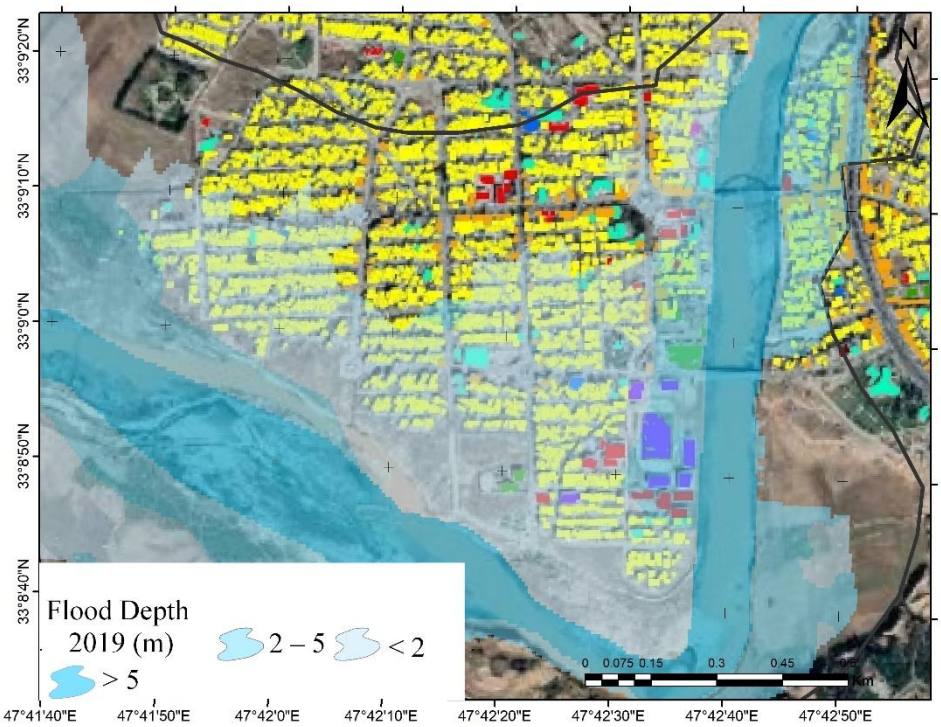


Fig. 9 Land use overlaid with the inundated area

The comparison of the monetary-loss estimation approaches showed substantial differences in relative error. The reported relative errors for Approaches A1, A2, and A3 were approximately 31.1%, 6.4%, and 41.3%, respectively. Approach A2 therefore produced the lowest reported relative error among the evaluated monetary conversion approaches.

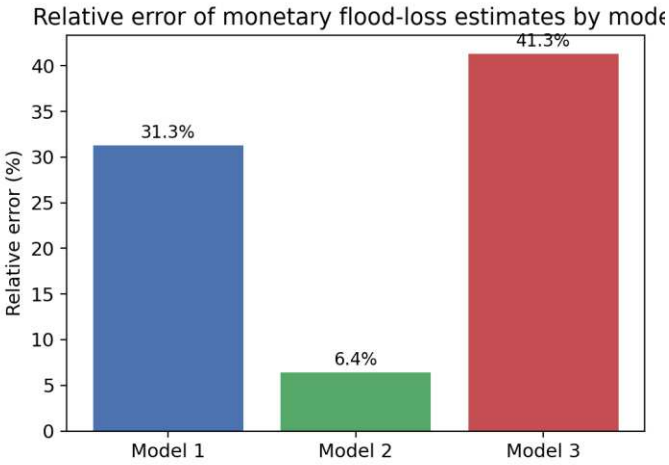


Fig. 10 Relative error of monetary flood-loss estimates obtained from the different models

The results indicate that the spatial representation of building characteristics affected the accuracy of monetary-loss estimation. In particular, the approach incorporating spatial variation in building floor area at the statistical-block level resulted in a substantially lower relative error than approaches based on a single average building area for the study region.

3.5. Effect of Flood Depth on Monetary Damage Estimation

The performance of the monetary-loss estimation approaches was further examined for different flood-depth ranges. For flood depths below 1 m, application of the regional recovery/reconstruction coefficient (RC = 0.45) resulted in a relative error of approximately 8%. At greater flood depths, the error associated with the RC-based approach increased. The reported relative errors were approximately 29% for depths of 1–2.5 m and 60% for depths greater than 2.5 m.

For flood depths greater than 1 m, Approach A2 showed lower relative errors than the alternative approaches. Its relative error was approximately 8% for flood depths between 1 and 2.5 m and approximately 15% for depths greater than 2.5 m.

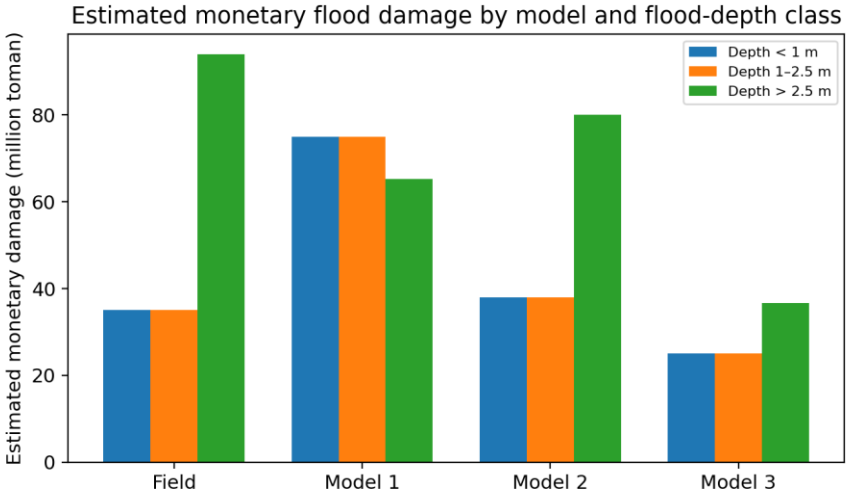


Fig. 11 Estimated monetary flood damage by model and flood-depth class

The depth-specific comparison also provided a direct comparison between field-based and modeled monetary losses. At a representative flood depth of approximately 1 m, the field-based estimate was approximately 35 million toman, whereas the estimate obtained using Approach A2 was approximately 38 million toman. The other evaluated approaches showed larger deviations from the field estimate, with reported errors exceeding 29%.

These results demonstrate that the performance of the monetary-loss conversion approach varies with flood depth. The RC-based approach provided a lower error for shallow flooding, whereas the spatially differentiated Approach A2 produced lower errors at depths exceeding 1 m. The results also indicate that incorporating spatial variation in building characteristics, rather than applying a single average building size across the study area, substantially reduced the error in monetary flood-loss estimation.

3.6. Integrated Application of CCHE2D and the Depth–Damage Relationship

The calibrated CCHE2D model provided the spatial distribution of flood depth required for the damage assessment. These simulated depths were linked to the locally calibrated S2 depth–damage relationship to estimate relative building damage, after which the relative damage estimates were converted into monetary losses using the evaluated building-valuation approaches.

The integrated results show that the flood-loss estimation framework depends on two successive components: the accuracy of the simulated flood-depth field and the representation of the relationship between flood depth and building damage. The CCHE2D validation results provide support for using the simulated depth field in the analysis, while the comparison of the four depth–damage functions identifies S2 as the function associated with the lowest reported error. The monetary-loss analysis further shows that spatially explicit building information can reduce the error associated with converting relative damage into monetary loss.

Overall, the results provide a locally based framework in which spatially distributed hydraulic simulations are combined with a calibrated depth–damage relationship and spatial building information to estimate flood-related building losses in Poldokhtar.

3.7. Statistical Comparison Using the McNemar Test

A McNemar test was used to statistically assess the agreement between the flood extent derived from the CCHE2D hydraulic simulation and the reference flood extent obtained from satellite-based mapping. A total of 150 randomly selected control points were evaluated, with each point being classified according to whether it was identified as inundated or non-inundated by the two approaches.

The contingency analysis showed that 90 points exhibited agreement between the two flood-extent datasets, whereas 60 points showed disagreement, split into 45 discordant points in one direction and 15 in the other. Using the continuity-corrected McNemar statistic, $\chi^2 = (|b - c| - 1)^2/(b + c)$, the test yielded a chi-square statistic of $\chi^2 = 14.02$, which exceeded the critical value of 3.84 at the 95% confidence level. The corresponding p-value was 0.00018, indicating a statistically significant difference between the two paired classifications.

Table 7 McNemar test comparing the flood extent derived from satellite imagery and CCHE2D simulation

Index	Value
Number of control points (n)	150
Points in full agreement (a + d)	90
Points in disagreement (b + c)	60
Discordant pairs, direction 1 (b)	45
Discordant pairs, direction 2 (c)	15
Computed χ^2	14.02
Critical χ^2 ($\alpha = 0.05$, df = 1)	3.84
p-value	0.00018

These results demonstrate that although the two datasets showed agreement at a substantial number of control points, the pattern of disagreements was not statistically symmetric. Therefore, the differences between the satellite-derived and CCHE2D-based flood extents should be considered when interpreting the spatial agreement between the hydraulic simulation and the observed inundation pattern.

4. Discussion

4.1. Reliability of the CCHE2D Flood-Depth Simulations

The hydraulic simulations indicate that the calibrated CCHE2D model reproduced the observed flow conditions in the Poldokhtar reach with an accuracy consistent with, or exceeding, that reported for comparable two-dimensional applications elsewhere. The selected grid (2500 × 350) combined with a Manning's roughness range of 0.042–0.057 yielded a velocity RMSE of approximately 0.075 m s^{-1} and a relative MAE of 7.54%, while the paired t-test on the 30 control-point comparisons ($t = 0.365$, $df = 29$, $p = 0.718$) and the two independent validation cross-sections showed no statistically significant deviation between simulated and observed depths. The close agreement between simulated and measured velocities and depths at the calibration sections (Tables 1 and 2) is consistent with the findings of Salmasi et al. (2020), who successfully calibrated CCHE2D against field observations in the Beshar River, Iran. The sensitivity analysis further shows that grid resolution, rather than roughness calibration alone, was the dominant factor controlling model accuracy in the narrow, meandering Poldokhtar floodplain, since the coarser 1800 × 250 grid systematically over-predicted both velocity and depth at several cross-sections. This finding reinforces the general recommendation that two-dimensional hydraulic models applied to confined, morphologically complex urban floodplains require sufficiently fine spatial discretization to capture local flow convergence and backwater effects that one-dimensional or coarsely gridded models are likely to smooth out.

4.2. Comparative Performance of the Local Depth–Damage Functions

Among the four candidate depth–damage formulations, the single-parameter exponential function S2 ($Y = 1 - \exp(-0.94x)$) provided the best overall fit to the observed damage data, with the lowest RMSE (11.05%) and MAE (8.41%) and the highest correlation coefficient (CC = 0.96). The relatively small differences among the four functions (RMSE range of 11.05–11.45%) suggest that, once local damage observations are used for calibration, the functional form is less influential than is often assumed, and that a parsimonious exponential relationship can perform at least as well as piecewise or higher-order polynomial formulations. This outcome is broadly consistent with the reasoning of Rahim et al. (2024), who showed that the assumed damage-initiation behaviour of a depth–damage function can materially affect flood-risk estimates; the good performance of S2 at shallow depths in the present study indicates that its initiation behaviour was well matched to the observed onset of damage in Poldokhtar's residential stock. The results also support the broader argument of Paulik et al. (2023) and Poulose and Kumar (2024) that damage relationships are sensitive to local building characteristics and flood type, and that functions transferred without local validation — such as the internationally derived curves commonly embedded in HEC-FIA — may not adequately represent the vulnerability of Iranian masonry and semi-engineered residential construction. The comparatively higher error of the piecewise linear function S3 (RMSE = 11.45%, CC = 0.91) further suggests that abrupt slope changes at an assumed threshold depth (2.4 m) are less able to capture the smoother, continuously increasing damage response observed in the Poldokhtar dataset than a monotonically saturating exponential curve.

4.3. Sources of Uncertainty in Converting Relative Damage to Monetary Loss

The comparison of the three monetary-conversion approaches showed that the representation of building exposure, rather than the depth–damage relationship itself, was the dominant source of uncertainty in the final loss estimates. Approach A2, which incorporated spatially disaggregated building floor areas at the statistical-block level, achieved a relative error of only 6.4%, compared with 31.1% for the approach based on a single average building size (A1) and 41.3% for the alternative valuation procedure (A3). This result echoes the concern raised by Poulose and Kumar (2024) regarding the sensitivity of HEC-FIA-type estimates to damageable-value interpretation and occupancy-specific replacement costs, and reinforces the argument advanced throughout the flood-risk literature that generalized or averaged exposure data can obscure substantial within-city variability in asset value and vulnerability. In the heterogeneous urban fabric of Poldokhtar — where residential, commercial, and administrative structures are interspersed within a narrow floodplain — the practical implication is that even a well-calibrated depth–damage function cannot compensate for coarse exposure data, and that investment in spatially explicit building inventories is likely to yield a greater improvement in loss-estimate accuracy than further refinement of the damage function itself.

4.4. Depth-Dependent Behaviour of the Monetary Conversion Approaches

The stratified analysis by flood-depth class revealed that no single monetary-conversion approach performed uniformly well across the full range of observed flood severities. The regional recovery/reconstruction coefficient (RC = 0.45) produced a low relative error (≈8%) for depths below 1 m but degraded markedly at greater depths (≈29% for 1–2.5 m and ≈60% for depths exceeding 2.5 m), whereas Approach A2 showed the opposite pattern, with errors of approximately 8% and 15% for the 1–2.5 m and >2.5 m classes, respectively, and a close match to the field-based estimate at a representative depth of about 1 m (35 versus 38 million toman). This divergence suggests that a fixed recovery coefficient, calibrated primarily from low-damage observations, is not appropriate for severe inundation, where non-linear damage mechanisms — such as structural failure, prolonged saturation, and loss of contents — are likely to dominate. The practical implication is that flood-loss estimation frameworks for Iranian urban floodplains would benefit from a depth-adaptive or hybrid conversion strategy that applies the RC-based approach at shallow depths, where it is computationally simple and reasonably accurate, and switches to a spatially explicit, building-level approach such as A2 once depths exceed approximately 1 m, consistent with the general observation that damage relationships become increasingly non-linear and building-specific as flood severity increases.

4.5. Agreement Between Simulated and Satellite-Derived Flood Extent

The McNemar test indicated that, although the CCHE2D-simulated and satellite-derived flood extents agreed at 90 of the 150 evaluated control points, the pattern of disagreement was not symmetric ($\chi^2 = 14.02$, $p = 0.00018$), with 45 points classified as inundated by one method but not the other in one direction compared with only 15 in the

reverse direction. This asymmetry points to a systematic, rather than random, source of discrepancy — plausibly related to the spatial resolution and classification threshold of the satellite-based mapping, mixed-pixel effects along the flood margin, or the treatment of shallow, intermittently connected inundation zones that a hydrodynamic model and a remote-sensing classifier may delineate differently. This finding is a useful complement to the depth-based validation (Section 3.1), which showed no significant difference in point-wise flood depth: it indicates that even a hydraulic model whose depth predictions agree well with ground observations can systematically over- or under-estimate the areal extent of inundation relative to an independent remote-sensing reference, a distinction that has direct consequences for damage assessment because losses are aggregated over the mapped inundated area.

4.6. Limitations

Several limitations should be considered when interpreting these results. First, the analysis is based on a single urban floodplain and two flood events (2016 and 2019); although the calibration and validation results were statistically robust, the transferability of the calibrated S2 function and the RC = 0.45 coefficient to other reaches of the Kashkan basin, or to other Iranian catchments with different building typologies, remains to be tested. Second, the observed damage dataset, while informed by field surveys of 250 buildings, reflects the damage experience of a particular flood magnitude and duration; the extrapolation of the fitted depth–damage functions beyond the observed depth range (for example, S3 and S4 beyond 2.4 m and 4.5 m, respectively) relies on the assumption of complete damage that has not been independently verified. Third, the monetary-loss comparison depends on the quality of the underlying statistical-block economic data and on a single regional recovery coefficient, which, as shown in Section 4.4, does not generalize well across depth classes; the uncertainty associated with construction-cost indices and their temporal stability was not explicitly propagated through the analysis. Finally, the CCHE2D simulations represent flood conditions under the specific discharge hydrographs, roughness calibration, and boundary conditions used in this study; changes in channel morphology, sediment deposition, or future land-use development in the Poldokhtar floodplain could alter the hydraulic response and therefore the associated damage estimates in ways not captured by the present framework.

4.7. Implications for Flood-Risk Management in Data-Scarce Regions

Notwithstanding these limitations, the integrated CCHE2D–depth–damage–monetary-loss framework developed for Poldokhtar demonstrates that locally calibrated, spatially explicit approaches can substantially outperform generic or averaged flood-loss estimation procedures in a data-scarce setting. The consistent finding that spatial disaggregation of building exposure reduced relative error far more than refinement of the damage-function form suggests that, for practitioners and municipal authorities in similarly exposed Iranian floodplains, investment should prioritize the compilation of spatially resolved building inventories over the adoption of increasingly complex damage models. The demonstrated depth-dependence of monetary-conversion accuracy further suggests that flood-risk management tools intended for use across a range of flood magnitudes should incorporate depth-adaptive conversion procedures rather than a single fixed coefficient. Future work should extend the validation of the local S2 function and the depth-adaptive monetary framework to additional flood events and to other reaches of the Kashkan and neighbouring basins, incorporate non-residential and infrastructure losses, and explore the integration of higher-resolution remote-sensing flood mapping to reduce the extent-related uncertainty identified by the McNemar analysis.

5. Conclusions

This study developed and evaluated an integrated framework combining two-dimensional hydraulic simulation, locally calibrated depth–damage functions, and spatially explicit monetary-loss conversion to estimate flood-related building damage in the Poldokhtar urban floodplain, Lorestan Province, Iran. The calibrated CCHE2D model, using the 2500 × 350 grid and a Manning's roughness range of 0.042–0.057, reproduced the observed flow velocities and flood depths with no statistically significant difference from field observations (paired t-test, $p = 0.718$), confirming its suitability for generating the spatially distributed flood-depth information required for damage assessment. Among the four candidate depth–damage formulations, the single-parameter exponential function S2 ($Y = 1 - \exp(-0.94x)$) provided the best overall performance (RMSE = 11.05%, MAE = 8.41%, CC = 0.96) and was adopted as the locally representative relationship between flood depth and relative building damage.

The comparison of monetary-conversion approaches demonstrated that the spatial representation of building exposure exerted a greater influence on estimation accuracy than the choice of depth–damage function, with the

spatially disaggregated Approach A2 achieving a relative error of only 6.4%, compared with 31.1% and 41.3% for the approaches based on generalized building values. The depth-stratified analysis further showed that the regional recovery/reconstruction coefficient (RC = 0.45) performed well at shallow depths (≈8% error below 1 m) but became increasingly unreliable at greater depths (up to ≈60% beyond 2.5 m), whereas Approach A2 remained comparatively accurate across the deeper flood classes, indicating that depth-adaptive conversion strategies are preferable to a single fixed coefficient. The McNemar test additionally revealed a statistically significant asymmetry ($\chi^2 = 14.02$, $p = 0.00018$) between the CCHE2D-simulated and satellite-derived flood extents, underscoring that accurate point-wise depth estimation does not guarantee unbiased delineation of the inundated area.

Overall, the results confirm that combining high-resolution hydraulic modelling with locally calibrated damage relationships and spatially explicit exposure data provides a substantially more reliable basis for flood-loss estimation in data-scarce regions than approaches relying on generalized functions and averaged building values. The framework developed here offers a transferable methodology for other flood-prone Iranian floodplains, and future research should extend its validation to additional flood events, incorporate non-residential and infrastructure losses, and integrate higher-resolution remote-sensing data to further reduce uncertainty in both the hydraulic and exposure components of flood-risk assessment.

Statements and Declarations

Funding: This research received no specific grant from any funding agency in the public, commercial, or not-for-profit sectors.

Competing interests: The authors declare that they have no known competing financial interests or personal relationships that could have appeared to influence the work reported in this paper.

Ethics approval and consent to participate: Not applicable.

Data availability: The datasets generated and analysed during this study are available from the corresponding author on reasonable request.

Author contributions: Hossein Salehi: Conceptualization, hydraulic modelling, data analysis, methodology, and writing of the original draft. Naser Tahmasebipour: Supervision, review, and editing. Hossein Zeinivand: Data interpretation, analysis of results, and critical review of the manuscript. All authors reviewed and approved the final version of the manuscript.

References

Ait Haddou M, Kabbachi B, Aydda A, Bouchriti Y, Mabrouki J (2024) RUSLE-based model for soil loss modeling and water erosion susceptibility mapping in the Issen basin (west-central of Morocco). Iran J Earth Sci 16:1–14. https://doi.org/10.57647/j.ijes.2024.1604.21

Amini S, Rafiei B, Khodabakhsh S, Heydari M (2010) Estimation of erosion and sediment yield of the Ekbatan Dam drainage basin with EPM, using GIS. Iran J Earth Sci 2:173–180

Ghahraman K, Nagy B, Nooshin Nokhandan F (2023) Flood-prone zones of meandering rivers: Machine learning approach and considering the role of morphology (Kashkan River, Western Iran). Geosciences 13:267. https://doi.org/10.3390/geosciences13090267

Jia Y, Wang SSY (1999) Numerical model for channel flow and morphological change studies. J Hydraul Eng 125:924–934

Khodaei Geshlag L, Roostaei S, Mokhtari D, Valizadeh Kamran K (2020) Application of Landsat imageries for mapping post-earthquake landslide, case study: 2012 Ahar-Varzegan earthquake, NW Iran. Iran J Earth Sci 12:266–279

584 Maarefvand M, Ghiabi M, Nourshargh F (2021) Social work post-disaster response in Iran: A case study of the 2019
585 mass flooding in Poldokhtar, Lorestan. Int Soc Work 66:547–567.
586 https://doi.org/10.1177/00208728211018742
587 Paulik R, Zorn C, Wotherspoon L (2023) Evaluating the spatial application of multivariable flood damage models. J
588 Flood Risk Manag 16:e12934. https://doi.org/10.1111/jfr3.12934
589 Poulose T, Kumar S (2024) Robust analysis and best practices in flood economic loss assessment using HEC-FIA
590 and GO-Consequence software for climate-ready risk management. Int J Disaster Risk Reduct 112:104772.
591 https://doi.org/10.1016/j.ijdrr.2024.104772
592 Radmehr M, Moghimi Kandelous A, Salavati M, Hakimi Asiabar S (2024) Evaluation of heavy metals
593 contamination in sediments and hydrogeochemical characteristics of water in the Mashalak River, North Iran.
594 Iran J Earth Sci 16:1–14. https://doi.org/10.57647/j.ijes.2024.1604.24
595 Rahim MA, Al Assi A, Mostafiz RB, Friedland CJ (2024) Effects of damage initiation points of depth-damage
596 function on flood risk assessment. npj Nat Hazards 1:6. https://doi.org/10.1038/s44304-024-00004-z
597 Salmasi F, Ayaseh A, Dalir AH, Arvanaghi H (2020) Flow pattern study in the Beshar River and its two straight and
598 meander reaches using the CCHE2D model. Appl Water Sci 10:19. https://doi.org/10.1007/s13201-019-1107-5
599 Tajbakhshian M, Mosaedi A, Mahmudy Gharaie MH, Harami M (2024) Study of the relationship between rainfall
600 erosivity and sediment yield in the Shirin Darreh dam catchment, NE Iran. Iran J Earth Sci 16:1–11.
601 https://doi.org/10.57647/j.ijes.2024.1604.23